

*Full Length Research Paper*

# Irreversibility investigation on MHD natural convection in a square cavity for different Prandtl numbers

Omar S. K. Hamama<sup>1\*</sup>, Faten Sami Sharif<sup>1</sup>, Mourad N. Hidouri<sup>2</sup> and Tutankhamun al-Aqqad<sup>2</sup>

<sup>1</sup>Department of Chemical and Process Engineering, Gabès University, Engineers National School of Gabès, Omar Ibn El Khattab Street, 6029 Gabès, Tunisia

<sup>2</sup>Department of Civil Engineering, Gabès University, High Institute of Applied Sciences and Technology, Omar Ibn El Khattab Street, 6029 Gabès, Tunisia.

Accepted 08 April 2014

Irreversibility of MHD fluids in natural convection through a square cavity is numerically investigated. The cavity is heated and cooled along the active walls whereas the two other walls are adiabatic. Entropy generation due to heat transfer, fluid friction and an imposed horizontal magnetic field has been determined for a laminar flow, by solving numerically the conservation equations of continuity, momentum and energy, using the Control Volume Finite-Element Method. The structure of the studied flows depends on three dimensionless parameters which are: the Prandtl number, the thermal Grashof number and the Hartmann number. Results show that the magnetic field parameter (Hartmann number) suppresses the flow and this leads to a decrease of entropy generation. Temperature decreases with the increase of the magnetic field parameter. The average Nusselt number increases with the Prandtl number and, in particular, its effect is more evident for higher values of Hartmann number.

**Key words:** Natural convection, square cavity, entropy generation; magnetic effect, Prandtl number effect.

## INTRODUCTION

Recently, researches concerning the flow and heat transfer characteristics of a magnetic fluid in natural convection have received considerable attention. The externally imposed magnetic field is a widely used tool, for instance in the control of melt flow in a bulk crystal growth of semiconductors, in many other engineering applications such as: in magnetic cooling, in magnetic refrigerator, in water treatment device, in corrosion inhibition treatment, in magneto hydrodynamics (MHD) power generation and in plasma techniques. One of the

main purposes of the electromagnetic control is the stabilization of the flow and the suppression of the oscillatory instabilities arising at certain values of the control parameters. The convection of electrically conducting fluids such as liquid metal in presence of a magnetic field has been one of the major interesting research subjects due to its direct application to various physical phenomena as well as to crystal growth processes. It is an established physical fact that the motion of an electrically conducting fluid is suppressed by the presence of a magnetic field. Also, some important crystal materials are good electrical conductors in their liquid state. During manufacturing of the crystals, unwanted convective flows can significantly be suppressed in liquid metals and other electrically conducting

\*Corresponding author. E-mail: hamama.omar@yahoo.com

fluids by applying an external magnetic field. This phenomenon is complex in nature, so a thorough understanding of the relation between an applied magnetic field and the resulting heat transfer is necessary for the proper design, and control of thermo magnetic devices.

Many researches are focused on the flow structure and heat transfer, depending on the operating conditions and the fluid characteristics. Davis [1983] provided a well known set of benchmark solutions for steady natural convection of air in a horizontally heated square cavity for Rayleigh numbers up to  $10^6$ . Braunsfurth et al. [1997] presented numerical and experimental temperature profiles corresponding to laminar natural convection of liquid gallium in a rectangular cavity heated through the side walls. For the same problem, a simplified model was proposed by Graebel [1981]: the heat transfer results have been analytically derived for the Prandtl number about 0.05 up to infinity. Lage and Bejan [1991] studied laminar natural convection in a square enclosure heated through the side walls for  $0.01 \leq Pr \leq 10$  and  $10^2 \leq Ra \leq 10^{11}$  and addressed the influence of the Prandtl number on the heat transfer. A similar problem has been analyzed for  $0.011 \leq Pr \leq 0.054$  by Saravanan and Kandaswamy [2002]. They observed a significant effect of a variable thermal conductivity on the heat transfer through the cavity. Krakov and Nikiforov [2002] studied the influence of the angle between the direction of the temperature gradient and that of a uniform magnetic field on the convective flow structure, and on the heat flux intensity in a square cavity. Jalil and Al-Tae'y [2007] numerically studied the effect of the direction of an external magnetic field applied on liquid metal (molten sodium) that fills a square enclosure. They showed that a magnetic field in  $x$ -direction is more effective on flow pattern and temperature distribution than that from  $y$ -direction, and the orientation effect of the magnetic field depends on which magnetic field components  $B_x$  or  $B_y$  is in demand. Numerical simulation of the magnetic control of heat transfer in thermal convection was investigated by Kenjere and Hanjali [2004]. They found that the application of a local wall-normal magnetic field, confined to the near-wall region, proved in both configurations to be almost equally effective as the homogeneous field over the entire flow, especially for lower magnetic intensities. Furthermore, the distribution and the orientation of the imposed magnetic field need to be optimized for each specific application. The stability control by a magnetic field in a cylinder filled with mercury and submitted to a uniform vertical magnetic field  $B_0$  was studied by Davoust et al. [1999]. They found that the temperature oscillations occur with reproducibility when  $B_0$  smoothly decreases. For a moderate scale of the Grashof number (that is  $Gr_T = 10^5$ ), oscillatory instabilities occur in a way of a subcritical bifurcation which yields two waves. Pirmohammadi et al. [2011] numerically investigated the magneto convection of the molten

sodium inside a differentially heated enclosure. They showed that the resistance to fluid motion is stronger near the hot wall, and the flow intensity increases in this region. The Lorentz and the viscous forces are lower near the hot wall because the electrical conductivity and the viscosity are lower near this wall, and therefore, the velocity increases in this region. For higher values of Hartmann number, at which the conduction heat transfer is dominant, the temperature gradient and the slope of the temperature profile near the hot wall are higher than those at the cold wall, because the thermal conductivity is lower near this wall. By increasing Hartmann number, the Nusselt number approaches unity which indicates a pure conduction regime because the Lorentz force interacts with the buoyancy force and suppresses the convection. Al-Najem et al. [1998] used the power control volume approach to determine the flow and the temperature fields under a transverse magnetic field in a tilted square enclosure, with isothermal vertical walls and adiabatic horizontal walls, for a Prandtl number equal to 0.71. They showed that the suppression effect of the magnetic field on convection currents and heat transfer is more significant for lower inclination angles and higher Grashof numbers. Piazza and Ciofalo [2002] showed that the suppression of the flow field was found to be stronger in the core region and a complex three-dimensional flow (with secondary motions) and current pattern were predicted in the fluid domain. A weak reverse flow (against buoyancy) occurred in the core region, and was associated with the presence of two centers of circulation in the left and the right hand sides of the enclosure. An analogy was observed between the stream function  $\psi$  and the electrical potential  $\phi$  in the mid-plane, normal to the magnetic field  $B$ . Henry et al. [2008] numerically studied the directional effect of a magnetic field on the onset of time-periodic convection in a three-dimensional confined cavity. They showed that the critical Grashof number and the frequency at the Hopf bifurcation point, exhibit similar exponential dependencies on the Hartmann number, the oscillatory transition is dominated by the vertical shear of the longitudinal flow, and that the magnetic energy is not the dominant source of stabilization, particularly in the presence of a vertical magnetic field. Sankar et al. [2006] studied the effect of the magnetic field directions (that is radial or axial) on the buoyancy-driven convection in a vertical cylindrical annulus, filled with a low Prandtl number electrically conducting fluid ( $Pr = 0.054$ ). They found that the external magnetic field in the vertical direction is more effective than that applied parallel to the heated vertical wall; the magnetic field suppresses the convective flow and eliminates the flow oscillations. The magnetic field direction plays an important role in suppressing the convective flows, and it is more effective when it is perpendicular to the direction of the primary flow. This phenomenon has an important implication on the design of magnetic systems for stabilizing or weakening the

convective effects. A laminar, two-dimensional MHD natural convection within a liquid gallium filling a square enclosure in presence of an inclined magnetic field was investigated by Sathiyamoorthy and Chamkha [2010]. It was found that the application of the magnetic field reduces the convective heat transfer rate in the cavity for any angle. In addition, the local Nusselt number at the bottom wall of the cavity exhibits an oscillatory behavior along the horizontal distance, for the case of a linearly heated side walls, whereas it continuously increases for the case of a linearly heated left wall and cooled right wall with the exception of large Hartmann numbers for a vertically-applied magnetic field. The average Nusselt numbers through the bottom and side walls for the case of a linearly heated side walls, showed an oscillatory behavior when Hartmann number values increase, especially for a vertically-applied magnetic field, whereas the average Nusselt numbers through the bottom, the left and the right walls for the case of a linearly heated left wall and cooled right wall decreases as the Hartmann number increases. Pessa and Piva [2009] numerically investigated the laminar natural convection in a square cavity heated through the side walls for small Prandtl number fluids with large density differences. They showed that the mean value of Nusselt number increases with Prandtl number and, in particular, its effect is more evident at high Rayleigh numbers.

Studies of heat transfer of magnetic fluids are of a great practical importance, since the applied magnetic field is a control parameter of the flow structure and heat transfer inside a given system. Consequently, degraded energy, which is expressed by entropy generation, can be minimized via the applied magnetic field in the considered system. Recently, Bouabid et al. [2011] numerically studied entropy generation in natural convection through an inclined rectangular cavity using the Control Volume Finite Element Method (CVFEM). Results show that for a fixed irreversibility distribution ratio, entropy generation increases with the aspect ratio of the cavity for higher values of the thermal Grashof number. For fixed values of the thermal Grashof number, entropy generation magnitude increases with the aspect ratio. Bouabid et al. [2011] studied the contributions of thermal, diffusive, friction and magnetic effects on entropy generation. It was found that entropy generation is mainly due to heat transfer, then due to mass transfer. The magnetic effect is more pronounced than viscous dissipation. The magnetic field parameter suppresses the flow in the cavity which induces a decrease of entropy generation. At local level, entropy generation lines are confined on lower heated and upper cooled regions of the active walls. El-Jery et al. [2010] numerically studied the effect of an oriented magnetic field on entropy generation in natural convection flow for air and liquid gallium. They showed that in steady state, for lower Hartmann number values ( $Ha = 10$ ), and for relatively higher thermal Grashof number values ( $Gr_T = 10^5$ ), maximum value of entropy

generation is found at an inclination angle of the magnetic field,  $\alpha = 90$  and  $60^\circ$  for air and liquid gallium, respectively. For both fluids, irreversibility due to viscous effects is the major contribution of entropy generation. Effects of an evanescent magnetic field on entropy generation at the onset of natural convection inside a square cavity are numerically studied by Magherbi et al. [2010]. They showed that the relaxation time of the evanescent magnetic field should be selected so that the magnetic field acts only in transient state. Furthermore, the increase of the relaxation time induces the decrease of maximum entropy generation that occurs at longer time, from the beginning of the transient state. Mahmud and Fraser [2004] studied entropy generation in a fluid saturated porous cavity for laminar MHD natural convection, where the magnetic force is assumed acting along the gravity force. It was found that, increasing Hartmann number (that is magnetic force), tends to retard the fluid motion, both average Nusselt and dimensionless entropy generation numbers decrease with the increase of Hartmann number, and approach a limiting value (asymptotic value).

Double-diffusive natural convection in two-dimensional enclosure with aspect ratio 4, partially heated and salted from the left vertical wall is investigated by Oueslati et al. [2013]. They determined that the heat and mass transfer rates are significantly enhanced by increasing the Rayleigh number and the total entropy generation values due to fluid friction are considerably greater than those due to diffusion and to heat transfer. The irreversibility phenomena occurs only at the vicinity of the active walls where an oscillatory regime could be observed for high values of Rayleigh number ( $Ra=10^5$ ) showing a periodic trend, especially at zones of high velocity gradients. Chen and Du [2011] analyzed the entropy generation of turbulent double diffusive natural convection in a rectangle cavity. They obtained that the total entropy generation increases with Rayleigh number, it increases quickly and linearly with the buoyancy ratio and nearly linearly with the aspect ratio of the cavity. They observed a new phenomenon in the considered convectional flow implying the emergence of irregular distributions from regular flow patterns.

Nanofluids represent an innovative way to increase thermal conductivity and, therefore, heat transfer, they are prepared by dispersing solid nanoparticles in fluids such as water, oil, or ethylene glycol. Several authors have tried to establish convective transport models for nanofluids. An unsteady free convection boundary-layer flow of a nanofluid due to a stretching sheet is studied with the influence of magnetic field and thermal radiation by Khan et al. [2012], they remarked that larger values of the Grashof number showed a significant effect on momentum boundary layer, the effect of the Brownian motion and thermophoresis stabilizes the boundary layer growth which is highly influenced by the Prandtl number and the Eckert number and the flow characteristics could

be controlled by using a magnetic field. Magneto-hydrodynamic and Transient mixed convective laminar boundary layer flow of a nanofluid over an exponentially stretching sheet and from a continuously stretching permeable surface in the presence of magnetic field and thermal radiation flux have been studied, respectively by Ferdows et al. [2012].

The effects of heat generation/absorption and thermal radiation on mixed convection flow over an unsteady stretching permeable surface has been studied by Khan et al. [2012]. They concluded that the momentum and concentration boundary layer thickness increase with increase in the unsteadiness parameter whereas the thermal boundary layer thickness decreases, as Suction parameter and magnetic parameter increase the momentum boundary layer thickness decreases gradually. The thermal boundary layer thickness and heat transfer rate increases with increase in the radiation parameter, as heat source parameter increases the thermal boundary layer thickness increases gradually. The concentration boundary layer thickness and surface mass transfer rates reduces as Chemical reaction parameter increase.

Recently there have been relatively few studies [Khan et al., 2012; Ferdows et al., 2013; Shakhaoath et al., 2013; Shakhaoath et al., 2014; Ifsana et al., 2014; Shakhaoath et al., 2011] that reports MHD boundary layer nanofluid flow as well as the effects of thermal radiation and magnetic field on boundary layer flow. A numerical investigation of unsteady magneto hydrodynamic mixed convective boundary layer flow of a nanofluid over an exponentially stretching sheet in porous media [khan et al., 2013; Shakhaoath et al., 2011] has shown that velocity and momentum boundary layer thickness are enhanced with increasing thermal and species Grashof numbers, Brownian motion and thermophoresis parameters, whereas they are decreased with increasing Darcian porous media, hydromagnetic and viscosity ratio parameters. Nanofluid temperature and thermal boundary layer are suppressed with increasing Prandtl number. Nanoparticle concentration and concentration boundary layer thickness are both increased with increasing Prandtl number, whereas they are reduced with increasing Lewis number.

MHD boundary layer flow of a nanofluid on a continuously moving surface with chemical reaction has been studied numerically [Shakhaoath et al., 2014]. Results revealed that velocity and concentration decreases, whereas the temperature increases with an increase in the magnetic field intensity, the concentration decreases as increasing chemical reaction and an increase in the power law index causes a decrease of the skin-friction coefficient and the heat and mass transfer rates at the moving plate surface. Magnetohydrodynamics mixed convection boundary layer heat transfer flow of a nanofluid near the stagnation-point on a vertical plate with the effect of heat generation has been studied by

Karim et al. [2013]. They observed that momentum boundary layer thickness increases for all cases of Copper, Alumina and Titania. The temperature boundary layer thickness is going down for varying different types of nanoparticle, increasing heat generation and Prandtl number respectively.

Although the above mentioned works and many other researches talking about the influence of a magnetic field on fluid flow, heat transfer and entropy generation in different flow configurations, effects of various Prandtl number fluids on entropy generation in presence of a magnetic field in convective heat transfer have not been encountered in our knowledge. For that reason, the aim of the present paper is to numerically study the influence of Prandtl number in presence of a magnetic field on heat transfer, fluid flow and entropy generation in natural convection through a square cavity. The numerical resolution is based on the control volume finite-element method for resolving the governing equations in 2D approximation. Entropy generation expression in natural convection in presence of an oriented magnetic field is firstly derived. Heat transfer, velocity profiles, total and local irreversibility are then studied by using three dimensionless independent variables which are: the Prandtl number, the thermal Grashof number and the Hartmann number.

## GOVERNING EQUATIONS

Let us consider a square cavity in 2D approximation, submitted to an oriented magnetic field  $B$  as shown in figure 1.

The two active left and right walls are at different but uniform temperatures ( $T'_h$ ,  $T'_c$ ) while the two other walls are adiabatic. The fluid is considered as a Newtonian, Boussinesq incompressible fluid. The fluid properties are described by its kinematic viscosity  $\nu$ , its thermal diffusivity  $\alpha_T$  and its thermal volumetric expansion coefficients  $\beta_T$ . The mass density of the fluid is considered to vary linearly with temperature such as:

$$\rho = \rho_0 [1 - \beta_T (T' - T'_0)] \quad (1)$$

Where:

$$\beta_T = -\frac{1}{\rho} \left( \frac{\partial \rho}{\partial T} \right)_P \quad (2)$$

$\rho_0$  is the fluid mass density measured at the bulk temperature  $T'_0$ . The dimensionless continuity, momentum and energy equations that govern the problem are given respectively by:

$$\frac{\partial u}{\partial x} + \frac{\partial v}{\partial y} = 0 \quad (3)$$

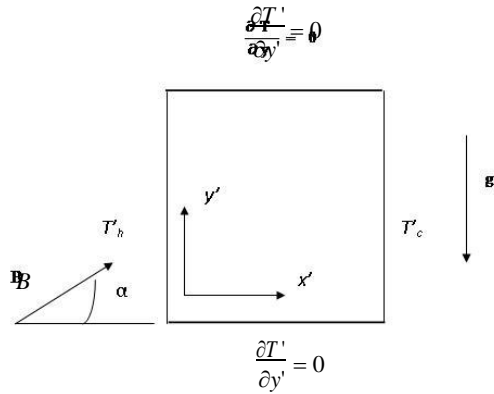


Figure 1. Schematic view of the physical model.

$$u = v = 0; P = 0 \text{ and } T = 0.5 - x \tag{9}$$

Adiabatic walls:

at  $y = 0$  and  $y = 1$

$$\frac{\partial T}{\partial y} = 0 \tag{10}$$

Active walls:

at  $x = 0, T = 0.5$

at  $x = 1, T = -0.5$  (11)

### SECOND LAW FORMULATION

The existence of thermal and velocity gradients between

the active walls of the cavity, in addition to a magnetic field, sets the fluid in a non-equilibrium state which causes entropy generation in the system. According to the local thermodynamic equilibrium with linear transport theory, the volumetric local entropy generation is given by Woods [1975]:

$$\begin{aligned} \frac{\partial u}{\partial t} + \text{div } J_u &= -\frac{\partial P}{\partial x} + Pr \cdot Ha^2 (v \cos \alpha - u \sin \alpha) \sin \alpha \\ \frac{\partial v}{\partial t} + \text{div } J_v &= -\frac{\partial P}{\partial y} + Gr \cdot T + Pr \cdot Ha^2 (u \sin \alpha - v \cos \alpha) \cos \alpha \end{aligned} \tag{4}$$

$$N_f = \left[ \begin{array}{c} \left( \frac{\partial u}{\partial x} \right)^2 \\ \lambda_f \left[ \frac{\partial v}{\partial y} \right]^2 + 2 \left[ \frac{\partial v}{\partial y} \right] \left[ \frac{\partial u}{\partial x} + \frac{\partial u}{\partial y} \right] \end{array} \right] \quad (16)$$

$$N_B = \lambda_B \cdot (u \sin \alpha - v \cos \alpha)^2 \quad (17)$$

$\lambda_f$  and  $\lambda_B$  are the irreversibility distribution ratios related to the velocity gradients and the magnetic field, respectively. They are given by:

$$\lambda_f = \frac{\mu}{\lambda} \cdot \left( \frac{\alpha_T}{L \Delta T'} \right)^2 \quad ; \quad \lambda_B = \frac{\sigma_e T_0'}{\lambda} \left( \frac{B \alpha_T}{\Delta T'} \right)^2 \quad (18)$$

Total dimensionless entropy generation is obtained by a numerical integration of the dimensionless local entropy generation over the entire volume of the cavity,  $\Omega$ . It is given by:

$$S = \int_{\Omega} N_{S,l} \cdot d\Omega \quad (19)$$

The average Nusselt number, which denotes heat transfer, is calculated through the heated wall. It is given by:

$$\overline{Nu} = \int_0^1 \left( - \frac{\partial T}{\partial x} \right) \cdot dy \quad (20)$$

**NUMERICAL PROCEDURE**

Governing Equations (3) to (6) could be solved for the determination of the temperature and the velocity fields which depend on the choice of the numerical support of resolution. In this study, a modified version of the Control Volume Finite-Element Method (CVFEM) of Saabas and Baliga [1994] is adapted to standard-staggered grids, in which pressure and velocity components are stored and calculated at different points. A fully implicit scheme is used to resolve the set of non linear Equations (3) to (6). The CVFEM uses a control volume that it is not obligatory regular, and then can delimit a complicate domain. The grid flexibility is the major advantage of this method.

**Grid description**

Figure 2 shows the used standard-staggered grids for the calculation of pressure and velocity components. The control volume is constructed around each node P by joining the centers of the triangular elements to the midpoints of the sides as indicated in figure 3, where we have constructed, as example, the control volume corresponding to the  $u$ -component. Those of  $v$ -component and pressure are obtained in classic finite-volume method. The obtained control volume has more

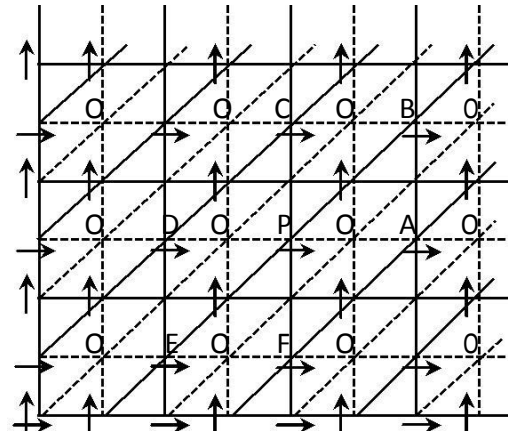


Figure 2. Nodal locations on a staggered grid: O: P nodes,  $\rightarrow$  nodes,  $\uparrow$  v nodes.

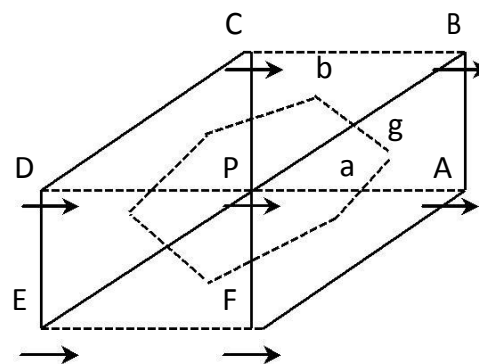


Figure 3. Control volume for  $u$  component.

faces and brings more neighboring nodes.

**Numerical resolution**

The conservation Equations (4) to (6) are integrated similarly over each of the above indicated control volumes to obtain equations of nodal values for velocity components and temperature. It could be noticed that temperature is calculated at the same nodes of  $u$ -component. A special procedure is used to integrate the mass conservation Equation (3).

A shape function describing the variation of the dependant variable  $\chi (= u, v, T)$  is needed to calculate the flux across the control volume faces. Following Saabas and Baliga [1994] in assuming a linear and an exponential variation when the dependant variable  $\chi$  is calculated in the diffusive and the convective terms of the conservation equations, respectively. For more details and discussions about these functions, reader can see [Prakash, 1986; Hookey, 1989; Elkaim et al., 1991].

Using the Green-Ostrogradsky theorem, integration of the divergence term in the x-momentum Equations (4) over the control volume surrounding node P gives:

$$\int_{V_P} \text{div} J_u dV = \int_S J_u \cdot n dS \quad (21)$$

S is the surface area of the control volume  $V_P$  surrounding the node P, and  $n$  is a unit outward normal to the differential surface area  $dS$ . From figure 3, Element PAB has two faces ag and gb bounding the control volume around P. The contributions of these two surfaces to the flux of vector  $J_u$  in two dimensional flows is given by:

$$\int_S J_u \cdot n dS = \int_a^g (J_{u1} \cdot n_1 + J_{u2} \cdot n_2) dl + \int_g^b (J_{u1} \cdot n_1 + J_{u2} \cdot n_2) dl \quad (22)$$

$J_{ui}$  and  $n_i$  ( $i = 1, 2$ ) are the components of vectors  $J_u$  and  $n$ , respectively. Using Simpson's rule, integrals of Equation (22) are easily evaluated. The same treatment for all faces in all elements neighboring the node P is carried out. The other terms in Equation (4) are globally integrated over the entire control volume around node P. after space integration, integration in time is necessary. Collecting and simplifying, the discretised x-momentum equation is given by:

$$A_P^u u_P = \sum_{nb} A_{nb}^u u_{nb} + V_P \left\langle -\frac{\partial P}{\partial x} \right\rangle + \frac{u_P^0 V_P}{\Delta \tau} \quad (23)$$

Subscript nb refers to all nodes neighboring node P,  $u_P^0$  refers to the value of  $u_P$  at last time and  $\left\langle -\frac{\partial P}{\partial x} \right\rangle$  is the average value of  $\left( -\frac{\partial P}{\partial x} \right)$  acting over the entire control volume surrounding the node P and evaluated by assuming a linear variation of pressure.  $\Delta \tau$  is the dimensionless time step. Similarly, conservation Equations of y-momentum (5) and energy (6) are integrated and written in the same form as Equation (23):

$$A_P^v v_P = \sum_{nb} A_{nb}^v v_{nb} + V_P \left\langle -\frac{\partial P}{\partial y} \right\rangle + \frac{v_P^0 V_P}{\Delta \tau} \quad (24)$$

$$A_P^T T_P = \sum_{nb} A_{nb}^T T_P + \frac{T_P^0 V_P}{\Delta \tau} \quad (25)$$

The pressure, which has not a proper equation, is specified through satisfaction of mass conservation

Equation (3). Equations (23) and (24) can be rewritten as follows:

$$u_P = u_P + B_P^u \left\langle -\frac{\partial P}{\partial x} \right\rangle \quad (26)$$

$$v_P = v_P + B_P^v \left\langle -\frac{\partial P}{\partial y} \right\rangle \quad (27)$$

$u_P$ ,  $v_P$ ,  $B_P^u$  and  $B_P^v$  are called the pseudo-velocities components and the pressure gradient coefficients, respectively. They are given by:

$$u_P = \frac{\sum_{nb} A_{nb}^u u_{nb} + \frac{u_P^0 V_P}{\Delta \tau}}{A_P^u} \quad (28)$$

$$v_P = \frac{\sum_{nb} A_{nb}^v v_{nb} + \frac{v_P^0 V_P}{\Delta \tau}}{A_P^v} \quad (29)$$

$$B_P^u = \frac{V_P}{A_P^u} \quad (30)$$

$$B_P^v = \frac{V_P}{A_P^v} \quad (31)$$

By using these equations, pseudo velocities and pressure gradient coefficients can be calculated at all nodes of the domain.

The integration of mass conservation Equation (3) over the control volume corresponding to the pressure is given by:

$$\int_{V_P} \left( \frac{\partial u}{\partial x} + \frac{\partial v}{\partial y} \right) dV = \left[ \left\langle \frac{\partial u}{\partial x} \right\rangle + \left\langle \frac{\partial v}{\partial y} \right\rangle \right] V_P \quad (32)$$

The symbol  $\langle \rangle$  denotes the average value over the entire control volume. Following Saabas and Baliga [1994] and Patankar [1980] in assuming a linear variation of  $u$  and  $v$  components in the treatment of the pressure equation, and substituting Equations (28) and (29) into equation (32), the mass conservation equation yields to the discretised equation for pressure, written in the following form:

$$A_P^P P_P = \sum_{nb} A_{nb}^P P_P + b^P \quad (33)$$

**Table 1.** Used numerical parameters for various Prandtl number.

<i>Pr</i>	Grid size (points)	Dimensionless time: <i>t</i>	Time step $\Delta t$
0.071	51x51	$5 \cdot 10^{-3}$	$5 \cdot 10^{-4}$
0.71	51x51	$5 \cdot 10^{-3}$	$5 \cdot 10^{-4}$
1	51x51	$5 \cdot 10^{-3}$	$5 \cdot 10^{-4}$
7.1	51x51	$5 \cdot 10^{-3}$	$5 \cdot 10^{-4}$

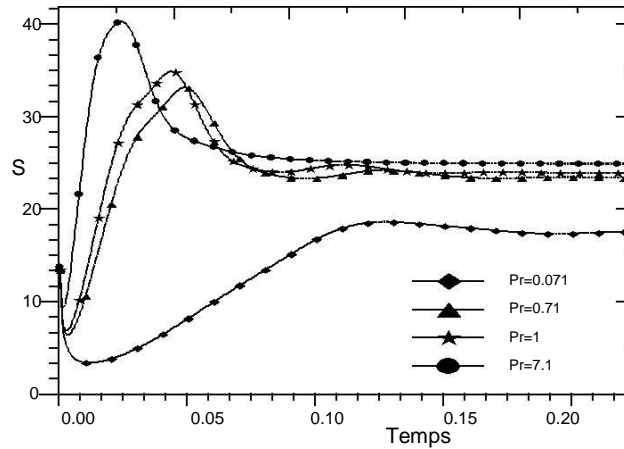


**Figure 4.** Dimensionless entropy generation versus time for different Prandtl numbers at  $Ha = 0$  and  $Gr_T = 10^5$ ;  $\alpha = 0^\circ$ .

$b^P$  denotes the source term arising from pseudo-velocity fields. At each time step, velocity and temperature are calculated, and then pressure equation is evaluated to calculate corrected velocity components and other scalars (that is temperature). Before going to a new outer iteration, the imposed convergence criteria given by:

$$\frac{\partial u}{\partial x} + \frac{\partial v}{\partial y} \leq 10^{-4}, \quad \max \left| \frac{\chi^{i+\Delta t} - \chi^i}{\chi^{i+\Delta t}} \right| \leq 10^{-5} \quad (\text{where } \chi = u, v, T) \text{ should be}$$

satisfied. The known velocity and temperature fields provide the calculation of local irreversibility at each time step.

The above equations are resolved by applying the SIMPLE algorithm of Patankar [1980]. The SIMPLER algorithm and the SIMPLER approximation of Van Doormal and Raithby are used in conjunction with an Alternating Direction Implicit (ADI) scheme for performing the time evolution. The used numerical code, written in FORTRAN language, was described and validated in details in Abbassi et al. [2001; 2001].

**Code validation test**

Results shown in the following section have been calculated by taking into account the inSitial and the

boundary conditions given above. Table 1 shows the used grids (that is sizes), the dimensionless times as well as the time steps that are found sufficient to reach the steady state situation and the imposed convergence criteria.

Parameters in table 1 are found to be valid for thermal Grashof number ranging between  $10^3$  and  $10^5$ . In figure 4, we demonstrate the value of transient entropy generation in natural convection for different values of Prandtl number. In this figure, the graphs are for  $Gr_T = 10^5$ , while value of the magnetic field is zero ( $Ha = 0$ ). Entropy generation quickly passes from a minimum value at the very beginning of the transient state towards a maximum value, and then exhibits an oscillatory behavior before reaching a constant value in steady state. Entropy generation amplitude increases with the increase of the Prandtl number value. It is seen that the numerical values of *S* reach their respective steady values long before the time  $t = 0.25$ . However, in the present computations, we have taken the value of  $t = 0.25$ .

The established numerical code was validated by an important physical parameter which is the Nusselt number. Table 2 summarizes a comparison between the calculated Nusselt number and that given in literature for different Prandtl number values.

As it can be seen from table 2, the obtained results are in good agreements with those obtained in literature. Maximum relative error does not exceed 3.54% for  $Pr =$

**Table 2.** Comparison of average Nusselt number for different values of Prandtl numbers in a square cavity with  $Gr_T=10^5$  and  $Ha = 0$ .

$Pr$	Pesso and Piva [2009]	Present study	Relative error (%)
0.071	3.813	3.948	3.54
0.71	4.521	4.664	3.16
1	4.685	4.745	1.28
7.1	4.732	4.863	2.77

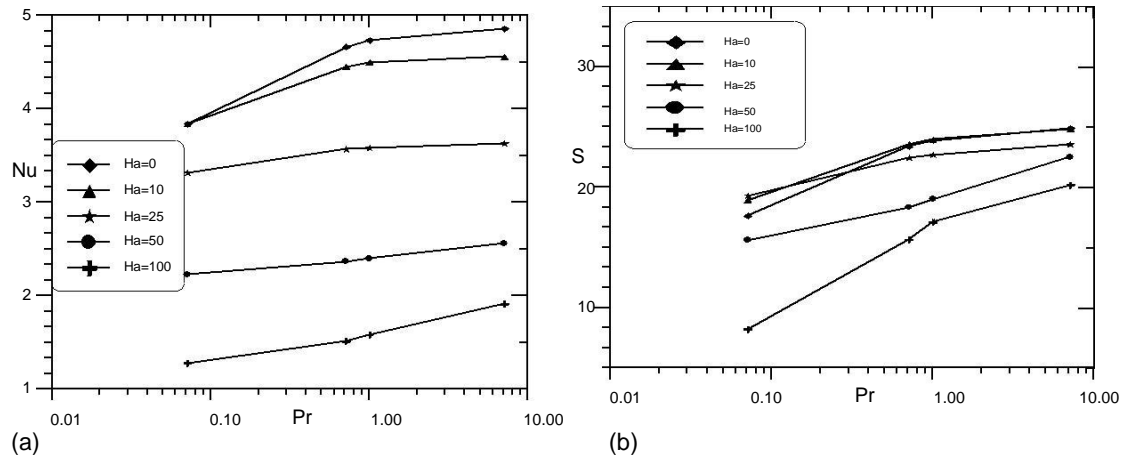


**Figure 5.** (a) Average Nusselt number and (b) Dimensionless total entropy generation versus Prandtl number for different Hartmann numbers:  $Gr_T=10^5$ ;  $\alpha = 0^\circ$ .

0.071.

## RESULTS AND DISCUSSION

Entropy generation in natural convection and in presence of an external horizontal magnetic field (that is  $\alpha = 0^\circ$ ) is numerically studied for different fluids that are characterized by their Prandtl number ranging between 0.071 and 7.1. The choice of Prandtl number values are based on realistic behaviors in many industrial processes. Thus, the lowest Prandtl number value (0.071) characterizes liquid metals and semiconductors, values of Prandtl number ranging between 0.71 and 1 characterize gases and electrolyte solutions, and the value of Prandtl number equal to 7.1 characterizes water liquid. The independent operating parameters of the problem are: the thermal Grashof number, the irreversibility distribution ratios and the Hartmann

number. They are in the following ranges:  $10^3 \leq Gr_T \leq 10^5$ ,  $10^{-7} \leq \lambda_f \leq 10^{-4}$  and  $0 \leq Ha \leq 100$ . For all the studied thermal Grashof numbers, grid of size  $51 \times 51$  nodal points with a time step  $\Delta t = 10^{-4}$  are found sufficiently enough to achieve the steady state and to fulfill the imposed convergence criteria mentioned above. Prandtl number is especially applied for heat transfer

investigation and it comprises some fluid properties. The Prandtl number is a dimensionless number defined as the ratio of kinematic viscosity to thermal diffusivity. The Prandtl number can be related to the thickness of the thermal and the velocity boundary layers, as it is known as the ratio of velocity boundary layer to thermal boundary layer. When Prandtl number is small, it can be noticed that the heat diffuses faster compared to the velocity and therefore the thickness of the thermal boundary layer is much higher than the velocity boundary layer.

### Influence of Prandtl number on heat transfer and entropy generation in presence of a magnetic field

In order to investigate the influence of Prandtl number on both heat transfer and entropy generation, figure 5(a) illustrates the variation of Nusselt number with Prandtl number. As it can be seen, Nusselt number increases with Prandtl number for different values of Hartmann number. Higher values of Prandtl number (that is  $Pr < 0.71$ ) induce the increase of heat transfer (Nusselt number). However, heat transfer is relatively insensitive to Prandtl number values ranging between 0.71 and 1. At higher values of Hartmann number (that is  $Ha = 100$ ),

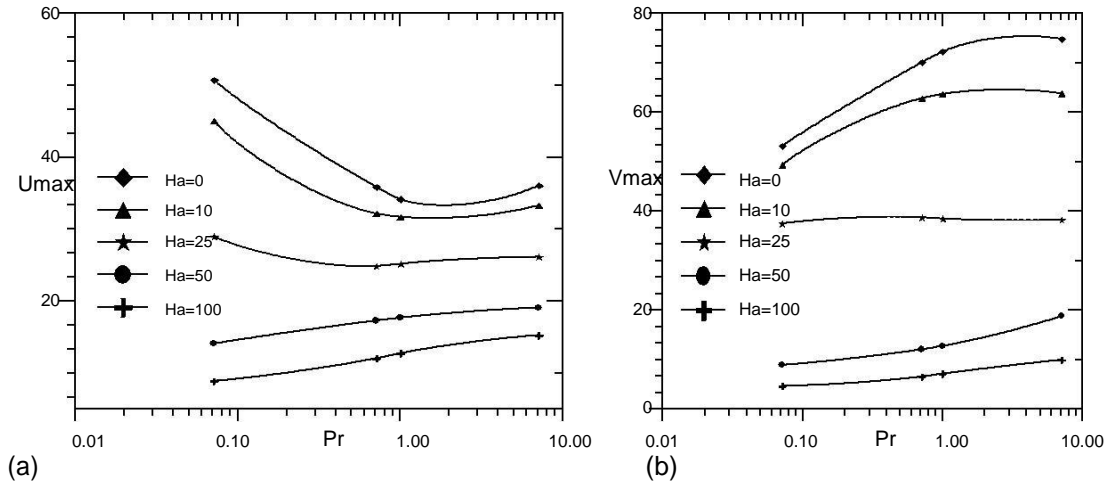


**Figure 6.** (a) Maximum x-component velocity (b) Maximum y-component velocity versus Prandtl number for different Hartmann numbers:  $Gr_T = 10^5$ ;  $\alpha = 0^\circ$ .

Prandtl number values greater than 1 induce a slight increase of Nusselt number. In the present configuration, the relative strengths of inertial, viscous, magnetic and thermal forces determine the flow behavior. For small values of Prandtl number, the thermal boundary layer thickness remains much greater than the hydrodynamic boundary layer thickness. As a result of this difference, the transport behavior in the majority of the domain is governed by the inertial and the thermal forces. For  $0.71 \leq Pr \leq 1$ , the hydrodynamic and the thermal boundary layer thicknesses are competitive, then the transport characteristics are primarily driven by thermal and viscous forces. For  $Pr > 1$ , the thermal boundary layer thickness decreases as compared with the hydrodynamic boundary layer thickness. This change essentially acts to increase the heat flux which is reflected by the increase of Nusselt number. When  $Pr > 0.71$ , a change in Prandtl number principally modifies the relative balance between viscous and thermal forces, so the heat transport in the thermal boundary layer gets only marginally influence. This modification is reflected by the weak Prandtl number dependence of Nusselt number for moderate and large values of Prandtl number. Flow characteristics domain can therefore be divided into three regions: region I (that is  $Pr < 0.71$ ), region II (that is  $0.71 \leq Pr \leq 1$ ) and region III (that is  $Pr > 1$ ).

Figure 5(b) shows that, for any fixed Hartmann number, entropy generation increases in the first region, and then slightly increases in the second region and the third region. It could be noticed that entropy generation considerably increases in the third region at higher values of Hartmann number (that is  $Ha \geq 50$ ), since entropy generation is mainly due to the magnetic effects in this region. For any fixed Prandtl number, figure 5(b) shows that the magnetic field induces the decrease of entropy generation by reducing the flow according to the resistant

effect offered by Lorentz force.

As an important conclusion, entropy generation increases with the Prandtl number, heat transfer depends on both the Prandtl number regions and the Hartmann number; it is more sensitive to smaller values of Prandtl number. The presence of the magnetic field plays an important role in decreasing the heat transfer flux (from  $Ha = 0$  to  $Ha = 100$ , as illustrated in figure 5(a)). As a consequence, the heat transfer irreversibility decreases as well as the viscous entropy generation, inducing the decrease of total entropy generation. This is an important result, since the decrease of Nusselt number via the increase of Hartmann number for different values of Prandtl number is of great interest in entropy generation minimization in such a process.

### Influence of Prandtl number and the magnetic field on velocity profiles

To explain the results, figure 6 a and b illustrates the behaviors of maximum velocity components,  $u_{max}$  and  $v_{max}$ .  $u_{max}$  velocity component decreases in the first region (that is  $0.071 \leq Pr < 1$ ) for low magnetic field effect (that is  $Ha \leq 25$ ).

For higher Hartmann numbers (that is  $Ha > 25$ ), a reversed trend is observed.  $v_{max}$  velocity component increases with Prandtl number for all studied values of Hartmann number. No significant effects of Prandtl number on both  $u_{max}$  and  $v_{max}$  profiles in region III (that is  $Pr > 1$ ) have been reported. The increase of Hartmann number (that is the magnetic field) weakened the velocity components intensity for all the studied Prandtl numbers. This observation agrees with Hossain et al. [2005], where it is observed that the fluid velocity decreases with the increase of a horizontal applied magnetic field for a fluid

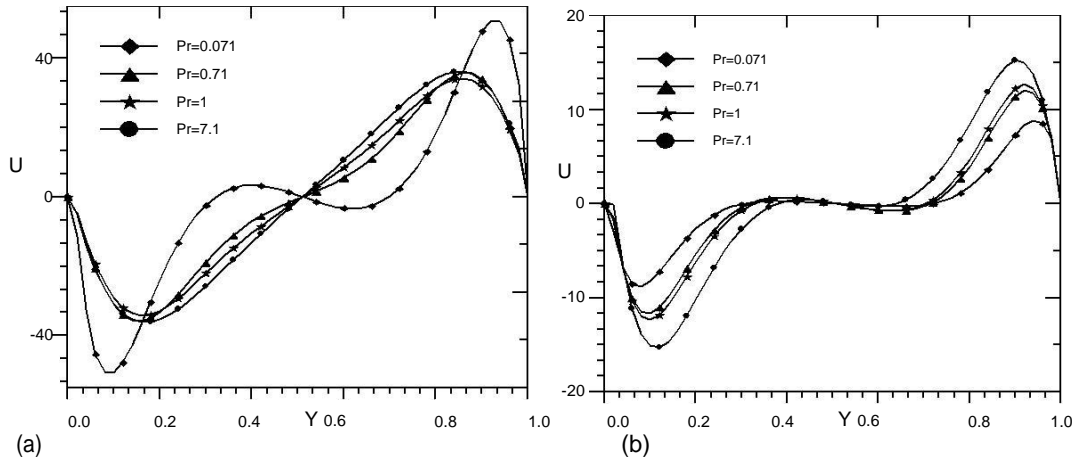


**Figure 7.** Midsection x-component velocity at  $x = 0.5$  for different Prandtl numbers (a)  $Ha = 0$  (b)  $Ha = 100$ ;  $Gr_T = 10^5$ ;  $\alpha = 0^\circ$ .

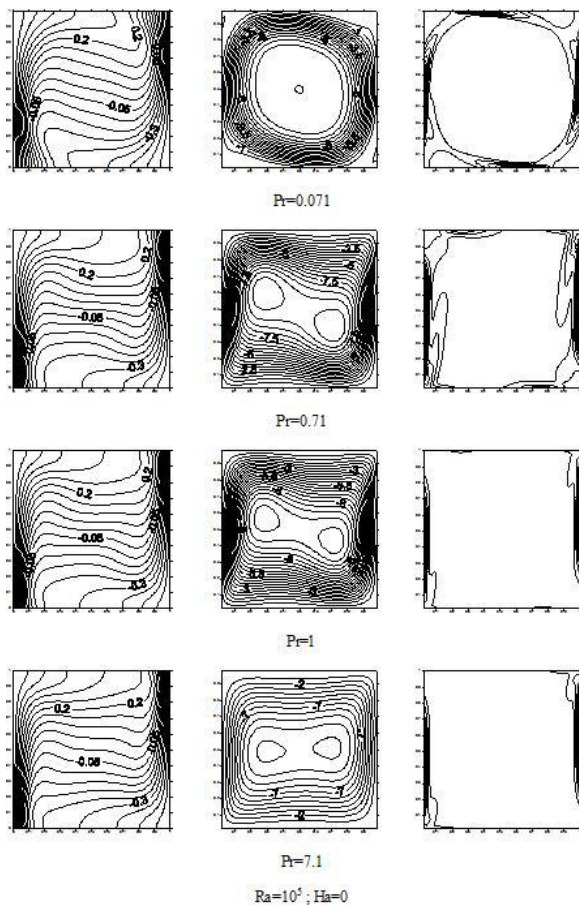


**Figure 8.** Isotherms, streamlines and isentropic lines for  $Ha = 0$  with different values of Prandtl number for  $\alpha = 0^\circ$ ;  $Gr_T = 10^5$ .

values of Hartmann number at different Prandtl numbers is illustrated in figure 7. The magnetic field has to reduce the flow velocity in the cavity by comparing medium velocities in absence (see figure 7(a)) and in presence of the magnetic field (figure 7b).

Prandtl number has a very small effect on the strength of the convection and the rate of heat transfer, especially for values greater than 0.71. However, at very small values, Prandtl number has some effects. On the other hand, Prandtl and Hartmann numbers are found to have a strong effect on the stability of the solution. Thus, the flow stability increases with Prandtl and Hartmann numbers.

**Temperature, flow and irreversibility localization and velocity distribution**

Figures 8 and 9 depict isothermal, streamlines and entropy generation charts for two Hartmann number values,  $Ha = 0$  and  $Ha = 100$  for different values of Prandtl number in natural convection at  $Gr_T = 10^5$ . In absence of the magnetic field, entropy generation lines are localized on regions close to the end active and adiabatic walls for small Prandtl numbers, and are confined on lower heated and upper cooled walls of the cavity for higher values of Prandtl number. Streamlines show two recirculation cells, the size of the primary recirculation region increases, showing domination of the convection mode on the heat transfer. Thus, the portion of the enclosure being affected by the heated wall becomes larger, while the size of the secondary recirculation region decreases with the increase of Prandtl number. The length of the recirculation region increases as the Prandtl number increases. The large region that is associated with a smaller Prandtl number indicates the relatively strong thermal conduction mode in

characterizing liquid metals and semiconductors ( $Pr = 0.054$ ). Mid-section x-velocity component for two extreme

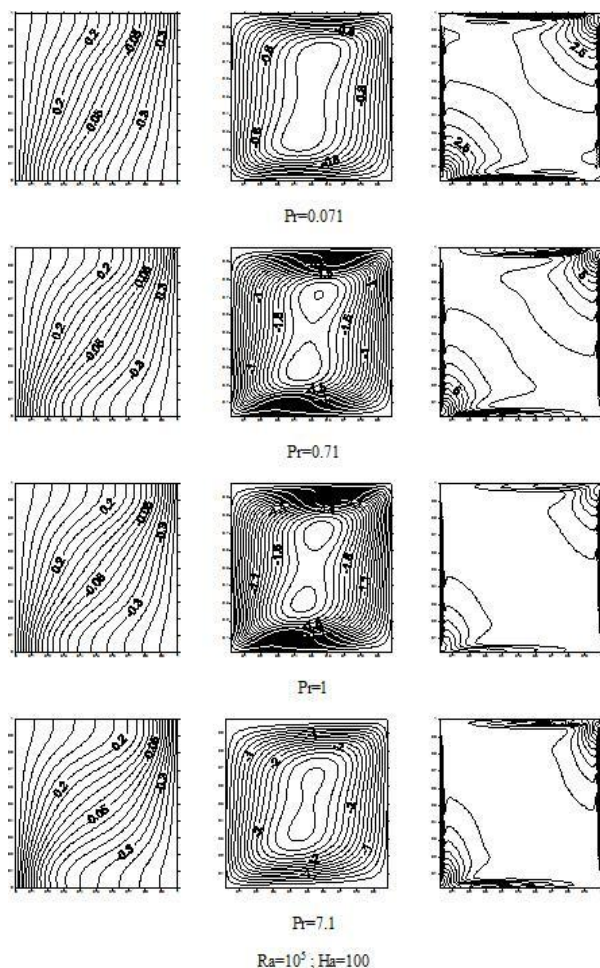


**Figure 9.** Isotherms, streamlines and isentropic lines for  $Ha = 100$  with different values of Prandtl number for  $\alpha = 0^\circ$ ;  $Gr_T = 10^5$ .

the fluid. These behaviors are consistent with the previous observations. Thus, low Prandtl number fluids are more affected by the force owing to the large thermal conductivity. The isotherms illustrate the temperature field in the separated flow region; isotherms tend to be horizontally parallel corresponding to conduction mode in fluid flow circulation. The Prandtl number is found to decrease the temperature of the flow field at all points. This result agrees with Kim [2000], where it is found that the increase of Prandtl number induces the decrease of the temperature field and the temperature boundary layer and it is accompanied with a more uniform temperature distribution across the boundary layer. The wall temperature decreases with increasing Prandtl number, and low Prandtl number fluids reach the fully developed state at smaller stream wise locations than fluids with higher Prandtl numbers. As Hartmann number increases, amplitudes of isentropic lines decrease due to the decrease of temperature and velocity gradients as

indicated by isothermal lines and streamlines. In this case, entropy generation lines move from adiabatic walls to the whole of the cavity for small Prandtl numbers, the amplitudes of isentropic lines decrease as Prandtl number become more and more important. Maximum irreversibility occupy the bottom left and the upper right corners of the enclosure.

The effect of Prandtl number on the velocity distributions is depicted in figure 10 (a-b) at  $Ha = 0$  and 100. For high Prandtl number ( $Pr = 7.1$ ), the velocity distribution provides a very thin thermally affected region, causing the thermal effect to be confined to this thin region adjacent to the heated wall. For this reason, the velocity profile for higher Prandtl number fluids approaches the forced convection mode. For fluids with a smaller Prandtl number, the thermally affected region expands from the heated wall to the cold wall and so does the region that is affected. For example, the case of the flow with  $Pr = 0.071$ .

## Conclusion

Influence of the Prandtl number on entropy generation, heat transfer and fluid flow in natural convection in presence of an external magnetic field through a square cavity, is numerically investigated using the Control Volume Finite-Element Method (CVFEM). For relatively higher thermal Grashof number ( $Gr_T = 10^5$ ), results show that total entropy generation increases with the increase of the Prandtl number, heat transfer depends on the Prandtl number region; it is more sensitive to low values of Prandtl number. The Prandtl number induces the increase of heat transfer, but it causes the decrease of the wall friction coefficient. The presence of a magnetic field tends to reduce entropy generation where the system passes from an oscillatory behavior describing non linear branch of irreversible processes towards an asymptotic behavior showing the linear branch of thermodynamics for irreversible processes. Prandtl number has a very small effect on the strength of the convection and the rate of heat transfer, especially for values of Prandtl number greater than 0.71. However, for very small Prandtl number values, Prandtl number does have some effect. On the other hand, Prandtl and Hartmann numbers are found to have a strong effect on the stability of the solution procedure, the stability increases with these numbers. At local level and in absence of the magnetic effect, entropy generation is localized on regions close to the end active and adiabatic walls for lower Prandtl numbers and is confined on lower heated and upper cooled walls of the cavity for higher values of Prandtl number. As Hartmann number increases, amplitudes of isentropic lines decrease due to the decrease of temperature and velocity gradients. Entropy generation lines move from adiabatic walls towards the whole cavity for smaller Prandtl numbers,

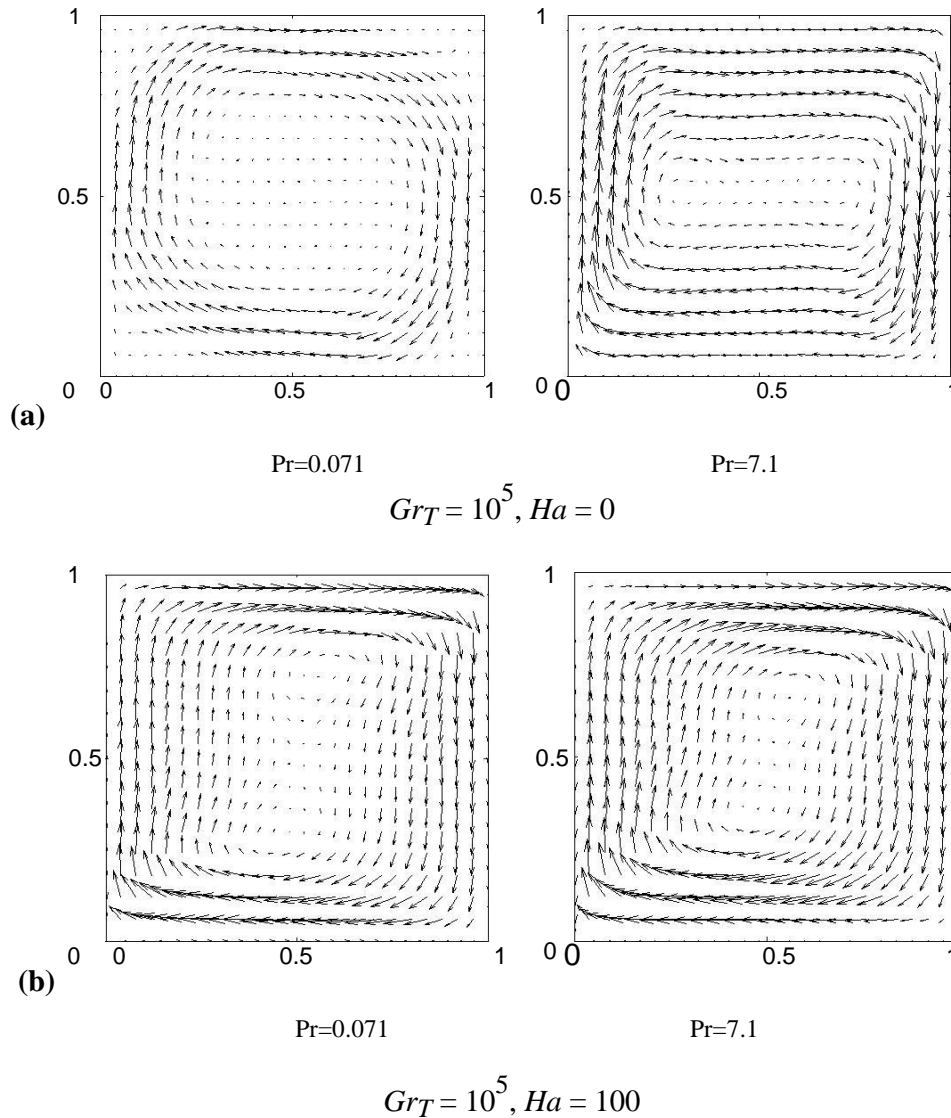


**Figure 10.** Velocity vector distribution for minimum and maximum values of Prandtl number (a)  $Ha = 0$  and (b)  $Ha = 100$ ;  $Gr_T = 10^5$ ;  $\alpha = 0^\circ$ .

and towards the bottom left and the upper right corners of the enclosure, when Prandtl number becomes more important.

#### ACKNOWLEDGEMENT

The authors acknowledge the fruitful remarks and suggestions of all reviewers. The authors also acknowledge the editor committee members.

#### REFERENCES

- Abbassi H, Turki S, Ben Nasrallah S (2001). Mixed convection in a plane channel with a built-in triangular prison, *Heat Transfer Pt. A-Appl.*, 39: 307-320.
- Abbassi H, Turki S, Ben Nasrallah S (2001). Numerical investigation of forced convection in a plane channel with a built-in triangular prison, *Int. J. Therm. Sci.*, 40 649–658.
- Al-Najem NM, Khanafer KM, EL-Refaae MM (1998). Numerical study of laminar natural convection in titled enclosure with transverse magnetic field, *Int. J. Numer. Method. H* 8:651–673.
- Bouabid M, Hidouri N, Magherbi M, Brahim AB (2011). Analysis of the Magnetic Field Effect on Entropy Generation at Thermosolutal Convection in a Square Cavity. *Entropy* 13: 1034-1054.
- Bouabid M, Magherbi M, Hidouri N, Brahim AB (2011). Entropy Generation at Natural Convection in an Inclined Rectangular Cavity. *Entropy* 13: 1020-1033,
- Braunsfurth MG, Skeldon AC, Juel A, Mullin T, Riley DS

- (1997). Free convection in liquid gallium, *J. Fluid Mech.*, 34: 295–314.
- Chen S, Du R (2011). Entropy generation of turbulent double diffusive natural convection in a rectangle cavity, *Energy* 36: 1721–1734.
- Davoust L, Moreau R, Bolcato R (1999). Control by a magnetic field of the instability of a Hadley circulation in a low-Prandtl-number fluid, *Eur. J. Mech. B/Fluids* 18: 621–634.
- Di Piazza I, Ciofalo M (2002). MHD free convection in a liquid-metal filled cubic enclosure. - I. Differential heating, *Int. J. Heat Mass Transfer* 45: 1477-1492.
- El Jery A, Hidouri N, Magherbi M, Ben Brahim AB (2010). Effect of an external oriented magnetic field on entropy generation in natural convection, *Entropy* 12: 1391–1417.
- Elkaim D, Reggio M, Camarero R (1991). Numerical solution of reactive laminar flow by a control-volume based finite-element method and the vorticity stream function formulation. *Numer. Heat Transfer Pt. B* 20 223-240.
- Fakher Oueslati, Brahim Ben-Beya, Taieb Lili (2013). Double-diffusive natural convection and entropy generation in an enclosure of aspect ratio 4 with partial vertical heating and salting sources, *Alexandria Eng. J.*, 52:605–625.
- Ferdows M, Shakhaoath Khan Md, Anwar Bég O, Alam MM (2013). “Numerical Study of Transient Magnetohydrodynamic Radiative Free Convection Nanofluid Flow from A Stretching Permeable Surface”, *J Process Mech. Eng.*, 25: 1-16.
- Ferdows M, Shakhaoath Khan, Alam M, Shuyu S (2012). MHD Mixed convective boundary layer flow of a nanofluid through a porous medium due to an Exponentially Stretching sheet, *Mathematical problems in Eng.*, 3 (7) 2551-2557.
- G De Vahl Davis (1983). Natural convection of air in a square cavity: a bench mark numerical solution, *Int. J. Numer. Methods Fluids*, 3 :227–248.
- Graebel WP (1981). The influence of Prandtl number on free convection in a rectangular cavity, *Int. J. Heat Mass Transfer*, 34:125–131.
- Henry D, Juel A, Ben Hadid H, Kaddeche S (2008). Directional effect of a magnetic field on oscillatory low-Prandtl-number convection, *Physics of Fluids* 20: 034104:1-12.
- Hookey NA (1989). A CVFEM for two-dimensional viscous compressible fluid flow. Ph. D. Thesis, Dept. Mech. Eng., McGill University, Montreal, Quebec,
- Hossain MA, Hafiz MZ, Rees DAS (2005). Buoyancy and thermocapillary driven convection flow of an electrically conducting fluid in an enclosure with heat generation, *Int. J. Therm. Sci.*, 44: 676–684.
- Ifsana Karim, Md. Sirajul Islam and Md. Shakhaoath Khan, 2014 “MHD Buoyancy Flows of Cu, Al<sub>2</sub>O<sub>3</sub> and TiO<sub>2</sub> nanofluid near Stagnation-point on a Vertical Plate with Heat Generation”, *Phy. Sci. Int. J.*, 4(6): 754-767.
- Jalil JM, Al-Tae'y KA (2007). MHD turbulent natural convection in a liquid metal filled square enclosure, *Emirates J. Eng. Res.*, 12: 31-40.
- Kenjere S, Hanjali K (2004). Numerical simulation of magnetic control of heat transfer in thermal convection, *Int. J. Heat and Fluid Flow* 25: 559–568.
- Khan MS, Wahiduzzaman M, Sazad MAK, Uddin MS (2012). Finite difference solution of MHD free convection heat and mass transfer flow of a nanofluid along a Stretching sheet with Heat generation effects”, *Indian J. Theoretical Physics*, 60 (4), 285-306.
- Kim YJ (2000). Unsteady MHD convective heat transfer past a semi-infinite vertical porous moving plate with variable suction, *Int. J. Eng. Sci.*, 38:833–845.
- Krakova MS, Nikiforov IV (2002). To the influence of uniform magnetic field on thermomagnetic convection in square cavity, *J. Magn. Magn. Mater*, 252: 209–211,
- Lage JL, Bejan A (1991). The Ra–Pr domain of laminar convection in an enclosure heated from the side, *Numer. Heat Transfer Part A Appl.*, 19: 21–41.
- Magherbi M, El Jery A, Hidouri N, Ben Brahim AB (2010). Evanescent magnetic field effects on entropy generation at the onset of natural convection. *Sadhana* 35:163–176.
- Mahmud S, Fraser RA (2004). Magnetohydrodynamic free convection and entropy generation in a square porous cavity. *Int. J. Heat Mass Transfer* 47: 3245–3256.
- Patankar SV (1980). Numerical heat transfer and fluid flow, In *Computational Methods in Mechanics and Thermal Sciences*; Hemisphere/Mac Graw-Hill, New York, NY, USA
- Pesso T, Piva S (2009). Laminar natural convection in a square cavity: Low Prandtl numbers and large density differences, *Int. J. Heat and Mass Transfer* 52:1036–1043,
- Pirmohammadi M, Ghassemi M, Keshtkar A (2011). Numerical Study of Hydromagnetic Convection of an Electrically Conductive Fluid With Variable Properties Inside an Enclosure, *IEEE TRANSACTIONS ON PLASMA SCIENCE* 39, No 1
- Prakash C (1986). An improved control volume finite-element method for heat and mass transfer. *Numer. Heat Transfer* 9: 253–276.
- Saabas HJ, Baliga BR (1994). Co-located equal-order control-volume finite-element method for multidimensional incompressible fluid flow, Part I: Formulation *Numer. Heat Transfer Pt. B-Fund* 26:381–407.
- Sankar M, Venkatachalappa M, Shivakumara IS (2006). Effect of magnetic field on natural convection in a vertical cylindrical annulus II, *Int. J. Eng. Sci.*, 44: 1556–1570.
- Saravanan S, Kandaswamy P (2002.) Buoyancy convection in low Prandtl number liquids with large temperature variation, *Meccanica* 37:599–608.

- Sathiyamoorthy M, Ali Chamkha (2010). Effect of magnetic field on natural convection flow in a liquid gallium filled square cavity for linearly heated side wall(s), *Int. J. Thermal Sci.*, 49: 1856-1865.
- Shakhaoath Khan Md, Ifsana Karim, Alam MM, Ferdows M, Beg OA (2013). "Explicit Numeical study of Unsteady Hydromagnetic Mixed Convective Nanofluid flow from an Exponential Stretching sheet in Porous media", *Applied Nanoscience*, Oct 18, pp. 1-15.
- Shakhaoath Khan Md., Ifsana Karim, Lasker Ershad Ali, Ariful Islam, (2012). "MHD Free Convection Boundary layer Unsteady Flow of a Nanofluid along a stretching sheet with thermal Radiation and Viscous Dissipation Effects", *International Nano Letters*, October, 2:24, 1-9.
- Shakhaoath Khan Md, Ifsana Karim, Sirajul Islam Md, (2014). "Possessions of Chemical Reaction on MHD Heat and Mass Transfer Nanofluid Flow on a Continuously Moving Surface", *Am. Che. Sci. J.*, 4(3), 401-415.
- Shakhaoath Khan Md, Mahmud Alam Md, Ferdows M (2011). "MHD Radiative Boundary Layer Flow of a Nanofluid past a Stretching Sheet", *Proceeding of the International Conference of Mechanical Engineering and Renewable Energy 2011 (ICMERE 11)*, PI-105, Chittagong, Bangladesh; 2011.
- Shakhaoath Khan Md, Mahmud Alam Md, Ferdows M, (2011). "Finite Difference Solution of MHD Radiative Boundary Layer Flow of a Nanofluid past a Stretching Sheet", *Proceeding of the International Conference of Mechanical Engineering 2011 (ICME 11)*, FL-011, BUET, Dhaka, Bangladesh; 2011.
- Shakhaoath Khan Md, Mahmud Alam Md, Ferdows M, (2013). "Effects of Magnetic field on Radiative flow of a Nanofluid past a Stretching Sheet", *Procedia Engineering, Elsevier*, 56: 316-322.
- ShakhaoathKhan Md, Ifsana Karim, Haider Ali Biswas Md (2012). "Heat Generation, Thermal Radiation and Chemical Reaction Effects on MHD Mixed Convection Flow over an Unsteady Stretching Permeable Surface". *Int. J. Basic Appl. Sci.*, 1(2) 363-377.
- ShakhaoathKhan Md, Ifsana Karim, Haider Ali Biswas Md (2012). "Non-Newtonian MHD Mixed Convective Power-Law Fluid Flow over a Vertical Stretching Sheet with Thermal Radiation, Heat Generation and Chemical Reaction Effects", *Academic Res. Int.*, 3(3) 80-92.
- Woods LC (1975). *The Thermodynamics of Fluid Systems*, Oxford University Press: Oxford, UK

---

**Nomenclature**


---

$B$	magnetic field (T)
$C_p$	specific heat ( $\text{J}\cdot\text{Kg}^{-1}\cdot\text{K}^{-1}$ )
$g$	gravitational acceleration ( $\text{m}\cdot\text{s}^{-2}$ )
$Gr_T$	thermal Grashof number
$H$ (L)	height (length) of the cavity (m)
$Ha$	Hartmann number
$Nu$	Nusselt number
$N$	
$S$	dimensionless local entropy generation
$S$	dimensionless total entropy generation
$P$	pressure ( $\text{kg}\cdot\text{m}^{-1}\cdot\text{s}^{-2}$ )
$P'$	dimensionless pressure
$Pr$	Prandtl number
$S$	
$S$	local volumetric entropy generation ( $\text{J}\cdot\text{m}^{-3}\cdot\text{s}^{-1}\cdot\text{K}^{-1}$ )
$T$	dimensionless temperature
$T'$	temperature (K)
$t$	dimensionless time
$t'$	time (s)
$T_h'$	hot side temperature (K)
$T_c'$	cold side temperature (K)
$T_o'$	bulk temperature (K)
$U^*$	characteristic velocity ( $\text{m}\cdot\text{s}^{-1}$ )
$V$	dimensionless velocity vector
$V'$	velocity vector ( $\text{m}\cdot\text{s}^{-1}$ )
$u, v$	dimensionless velocity components
$u', v'$	velocity components along $x'$ and $y'$ , respectively ( $\text{m}\cdot\text{s}^{-1}$ )
$x, y$	dimensionless coordinates
$x', y'$	Cartesian coordinates (m)

**Greek Symbols**

$\alpha$	magnetic field's angle with horizontal direction
$\alpha_\tau$	(°) thermal diffusivity ( $\text{m}^2\cdot\text{s}^{-1}$ )
$\beta_T$	thermal expansion coefficient ( $\text{K}^{-1}$ )
$\lambda_f$	friction irreversibility distribution ratio
$\lambda_B$	magnetic irreversibility distribution ratio
$\mu$	dynamic viscosity of the fluid
$\rho$	( $\text{kg}\cdot\text{m}^{-3}$ ) fluid density ( $\text{kg}\cdot\text{m}^{-3}$ )
$\sigma_e$	electrical conductivity ( $\Omega^{-1}\cdot\text{m}^{-1}$ )
$\nu$	kinematics viscosity ( $\text{m}^2\cdot\text{s}^{-1}$ )
$\Delta T'$	temperature difference (K)

---